

Deep Roto-Translation Scattering for Object Classification

Edouard Oyallon and Stéphane Mallat
Département Informatique, Ecole Normale Supérieure
45 rue d'Ulm, 75005 Paris
edouard.oyallon@ens.fr

Abstract

Dictionary learning algorithms or supervised deep convolution networks have considerably improved the efficiency of predefined feature representations such as SIFT. We introduce a deep scattering convolution network, with complex wavelet filters over spatial and angular variables. This representation brings an important improvement to results previously obtained with predefined features over object image databases such as Caltech and CIFAR. The resulting accuracy is comparable to results obtained with unsupervised deep learning and dictionary based representations. This shows that refining image representations by using geometric priors is a promising direction to improve image classification and its understanding.

1. Introduction

Learning image representations has considerably enhanced image classification results compared to geometric features such as edge descriptors, or, SIFT and HOG [19, 7] patch representations. Learning may thus seem to be a more promising direction for improving image analysis rather than refining geometric image analysis. This paper aims at showing that understanding how to take advantage of geometrical image properties can define image representations, providing competitive results with state of the art unsupervised learning algorithms. It shows that refining geometric image understanding remains highly promising for image classification.

Supervised deep neural network learning achieves state-of-the-art results on many databases [11, 16]. However, several works [30, 8] have shown that the Alex-net [11] trained on ImageNet still performs very well on different databases such as Caltech or PASCAL VOC. The output of this neural network can thus be considered as a “super SIFT” image descriptor, which is used as an input to a linear SVM classifier [30, 8]. It indicates that this deep network is capturing important generic image properties, which are not dependent upon the classes used for training. In the same

spirit, unsupervised deep learning [13] as well as unsupervised bag of words [26] or dictionary learning with spatial pyramid [12] have improved classification results previously obtained with engineered feature vectors such as SIFT or HOG, on complex object recognition databases. However, these unsupervised learning algorithms are tailored to each databases. One may wonder whether their improved performances result from an adaptation to the specific properties of each databases, or whether these unsupervised representations capture refined geometric image properties compared to SIFT or HOG features.

A scattering convolution network is constructed with predefined complex wavelet filters, which are adapted to geometric image variabilities [22]. It provides a mathematical and algorithmic framework to incorporate refined geometric image priors within the representation. Since images are projections of 3D scenes under various view points, the main source of geometric image variabilities comes from rigid movements, and deformations resulting from perspective projections. An important issue is to build adaptive invariants to these sources of variability, which preserve essential information to discriminate different classes. A translation invariant scattering network was studied in [5] for digit image classification and texture recognition, but which was not powerful enough to classify complex objects as in Caltech or CIFAR. A translation and rotation invariant deep scattering network was introduced in [25] to classify textures with strong rotations and scalings. However, imposing rotation invariance is a prior which is too strong for image object and scene classifications, which are typically not fully rotation invariant.

Section 2 introduces a scattering representation which is translation invariant, and which efficiently represents rotation variability without imposing full rotation invariance. It yields a representation which complements SIFT type coefficients, with coefficients incorporating interactions between scales and angles. This roto-translation scattering representation is nearly complete in the sense that good quality images can be recovered from roto-translation scattering coefficients [4]. It is also stable to additive perturba-

tions and small deformations, which guarantees to avoid the type of instability observed in some deep networks [28]. In this architecture, the loss of information only appears at the final supervised classification stage, which computes invariants adapted to the classification task. It includes an orthogonal least square supervised feature selection followed by a linear or a Gaussian kernel SVM.

This scattering representation is tested in Section 4 over Caltech and CIFAR data bases for object classification. It yields results which are well above all other representation which do not incorporate any learning, based on SIFT type features or with random weight deep networks. It also gives competitive results with state of the art unsupervised learning procedure adapted to each databases, which indicates that these unsupervised learning algorithm do not capture geometric transformations which are more powerful than rigid movements and small deformations. Computations can be reproduced with a software that is available at <http://www.di.ens.fr/data/software>.

2. Roto-Translation Scattering Networks

Images have important geometric variability due to perspective projections of 3D scenes under various viewpoints. It includes a combination of rigid movements and deformations. This section introduces a separable scattering transform, which constructs a nearly complete representation, based on elementary features, which linearizes important geometric variability. This representation is used for object classification. Scattering networks are particular classes of convolution networks [22], whose filters are computed with wavelets. They are introduced in the framework of convolution networks to better understand the specificities of their architecture.

2.1. Convolution Network Cascade

A convolutional network is a multilayer architecture, which cascades spatial convolutions and pooling operators, which includes sub-samplings [15]. These networks compute progressively more invariant image descriptors over multiple layers indexed by $0 \leq j \leq J$.

For $j = 0$, the network illustrated in Figure 1 takes in input an image x of P pixels, with potentially $Q_0 = 3$ color frames. For $j > 0$, each layer $x_j(p, q)$ is a set of Q_j image frames, which correspond to different “feature types” indexed by $1 \leq q \leq Q_j$. Each feature image has P_j pixels indexed by p . It is computed from x_{j-1} by applying a linear operator F_j to x_{j-1} , followed by a non-linearity, which may be a rectifier, a thresholding, a modulus or some other nonlinearities “pooling” functions [15]. Convolution networks impose that for each fixed q , F_j computes a convolution of $x_{j-1}(p, q)$ along p , with a filter which depends upon q . The operator F_j also linearly combines the Q_{j-1} image frames of x_{j-1} indexed by q . The output vector $F_j x_{j-1}$ is then

transformed by a non-linear “pooling operator” which may incorporate a rectifier, a modulus, a thresholding [15]. For scattering transforms, $F_j x_{j-1}$ is a complex valued signal and the non-linearity is a complex modulus, so we write:

$$x_j = |F_j| x_{j-1}. \quad (1)$$

Figure 1 illustrates this computational architecture introduced by LeCun [15].

The operators $|F_j|$ progressively propagate x across the network until the last layer x_J . The cascade of convolutions produce operators of progressively wider supports as j increase. The depth j thus corresponds to a scale index of the non-linear network features. A classifier is applied to the output x_J . It may be a linear SVM, a RBF network, or some other fully connected double layer classification networks [11, 15]. In our numerical experiments, we use a dimensionality reduction step followed by a Gaussian SVM.

The network architecture is specified by the dimensions $P_j \times Q_j$ of each layer and by the non-linear pooling operator. This is a delicate step, which is usually done through an ad-hoc engineering trial and error process. Given this architecture, one must then optimize each operators F_j to achieve a low classification error. Experiments have been performed with random weights [24]. Better results are however obtained with unsupervised training of the weights, using auto-encoders [29]. When enough labeled examples are available, even better results are obtained with supervised training algorithms which back-propagates classification errors [14]. The Alex-Net is an example of supervised deep network trained with labeled images of the ImageNet data basis [11].

2.2. Scattering Network

A scattering network is a convolutional network whose architecture and filters are not learned, but are predefined wavelets. These wavelets are adapted to the type of geometric invariants and linearization that need to be computed. Image classification typically requires to build image features which are locally invariant to translations and stable to deformations. It should thus linearize small deformations so that these deformations can be taken into account or removed with a linear operator, which is adjusted by the final supervised classifier.

Scattering networks compute inner-layer coefficients $x_j(p, q)$, which are nearly invariant to translations of the input image x by less than 2^j . Each image frame is sub-sampled at intervals 2^{j-1} . The factor 2 oversampling avoids aliasing phenomena. If x has P pixels then each network layer x_j has Q_j frames of $P_j = P 2^{-2j+2}$ pixels. The size Q_j does not result from an ad-hoc decision but depends upon the choice of geometric invariant as we shall see.

It has been proved mathematically that translation invariance and linearization of deformations is obtained with

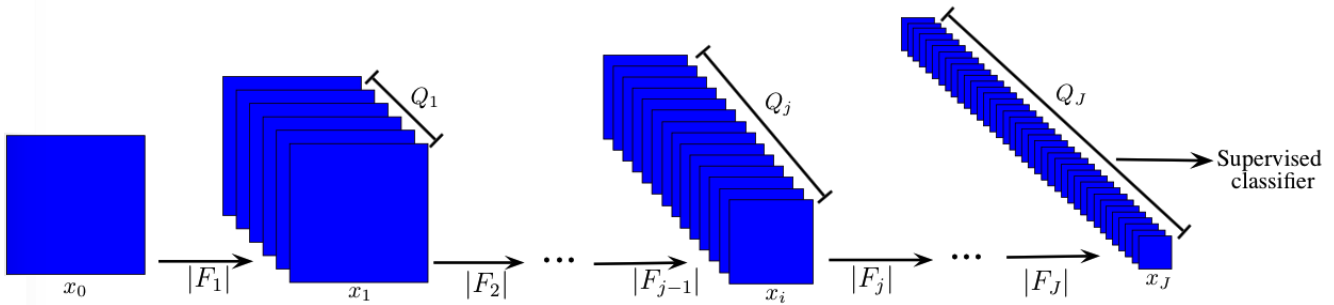


Figure 1. A convolution network computes a layer x_j by applying a linear operator F_j to x_{j-1} , followed by a non-linearity which we choose to be a modulus.

wavelets [22]. They separate the image information along multiple scales and orientations. Cascading wavelet transforms and modulus non-linearities lead to translation invariant scattering transforms [22], which have been applied to digit and texture classifications [5]. Rotation invariant scattering networks have been introduced by replacing wavelet spatial convolutions by convolutions along the special Euclidean group of rigid movements. It takes into account both translations and rotations [25]. We introduce a simpler separable convolution, which still has the ability to build invariants over rigid movements, but which leaves the choice of invariant to the final SVM classifier.

Wavelet transforms can be computed with a cascade of linear filtering and sub-sampling operators, which are called multi-rate filter banks [21]. Although deep networks apply non-linearities at each layer, they also include such linear cascades. Indeed, rectifier or modulus non-linearities have no impact over positive coefficients, produced by averaging filters in the network. All non-linearities can thus be removed from averaging filters output. Deep network computations can therefore be factorized, as cascades of $j - 1$ averaging and sub-sampling operators, followed by a band-pass filter and a non-linearity, for multiple values of j . If the network includes a sub-sampling by a factor 2 at each layer, then this is equivalent to a convolution with multiple wavelets of scale 2^j , and a non-linearity. These cascades are followed by new cascades of $k - 1$ averaging operators, for different k , followed by a band-pass filter and a non-linearity, and so on. This is equivalent to convolutions with a second set of wavelets of scale 2^{j+k} , and a non-linearity. The scales depend upon the number of averaging and sub-samplings along each network path, and thus satisfy $1 \leq j + k \leq J$.

In the following, we describe a second order scattering transform operator S_J , which performs at most two wavelet convolutions. The network output x_J is computed with a first 2D spatial wavelet transform W_1 which performs spatial wavelet image convolutions whose phase are removed by a non-linear modulus. We then apply a second wavelet transform W_2 , which is adapted to the desired

invariants, not only along translations but also along rotations. This is done by computing separable 2D convolutions with wavelets along space, and 1D convolutions with wavelet along angle variables. The output is averaged by an operator A_J which performs a spatial averaging at the scale 2^J :

$$x_J = S_J x = A_J |W_2| |W_1| x .$$

Higher order scattering transforms are obtained by cascading more wavelet transforms, which can be adapted to other group of transformations. However, this paper concentrates on second order scattering along space and rotation variable. This second order should not be confused with the network depth J , which corresponds to the maximum spatial invariance scale 2^J , and typically depends upon the image size. Next two sections describe the implementations of the two wavelet transforms W_1 and W_2 and the averaging operator A_J .

2.3. Spatial Wavelet Transform W_1

The first wavelet transform W_1 separates the image component along different scales and orientations, by filtering the image x with a family of wavelet $\psi_{j,\theta}$. These wavelets are obtained by dilating by 2^j a mother wavelet $\psi(p)$, and rotating its support with r_θ along L angles θ :

$$\psi_{j,\theta}(p) = 2^{-2j} \psi(2^{-j} r_\theta p) \text{ for } \theta = \frac{\ell\pi}{L} .$$

As in [5, 25], we choose a complex Morlet wavelet ψ which is a Gaussian modulated by a complex exponential, to which is subtracted a Gaussian to set its average to zero. Figure 2 shows the real and imaginary parts of Morlet wavelets along $L = 8$ angles. The modulus computes the envelop of complex wavelet coefficients, sub-sampled at intervals 2^{j-1} . Coefficients at the scale 2^j are stored at the depth j :

$$x_j^1(p, \theta) = |x \star \psi_{j,\theta}(2^{j-1} p)| .$$

These coefficients are nearly invariant to a translation of x smaller than 2^j . For $2^j < 2^J$, this invariance will be improved by further propagating these coefficients up to layer

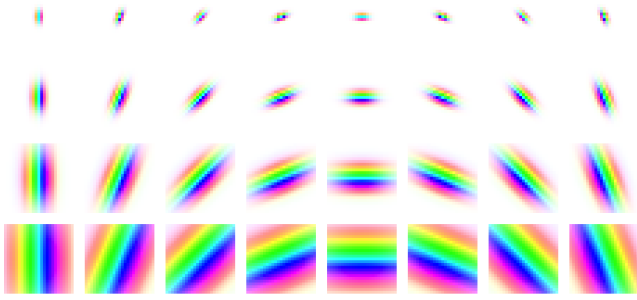


Figure 2. Real and imaginary parts of Morlet wavelets at different scales 2^j for $1 \leq j \leq 4$ and $L = 8$ orientations. Phase and amplitude are respectively given by the color and the contrast.(best viewed in color)

J , with a second wavelet transform described in the next section.

Coefficients at the scale 2^j correspond to deep network coefficients of depth j because in a deep network they are calculated by cascading $j - 1$ low-pass filters, and a final band-pass filter. The cascade of low-pass filters defines a pyramid of low-passed images $x \star \phi_j$, where ϕ_j is a scaled low-pass filter:

$$\phi_j(p) = 2^{-2j} \phi(2^{-j}p).$$

Each $x \star \phi_j$ is computed by convolving $x \star \phi_{j-1}$ with a low-pass filter h followed by a sub-sampling. It is stored as an image indexed by $q = 0$ in the layer j :

$$x_j^1(p, 0) = x \star \phi_j(p) = h \star (x \star \phi_{j-1})(2p). \quad (2)$$

Applying a modulus has no effect because these coefficients are positive. The wavelet coefficients $x \star \psi_{j,\theta}$ are computed by applying a complex band-pass filter g_θ followed by a sub-sampling. In this case, the modulus has a strong impact by eliminating the complex phase. It is stored as an image indexed by $q = \theta$ in the layer j :

$$x_j^1(p, \theta) = |x \star \psi_{j,\theta}(p)| = |g_\theta \star (x \star \phi_{j-1})(p)|. \quad (3)$$

The wavelet transform W_1 is thus implemented in a deep network calculated with a cascade of low-pass and band-pass filtering, followed by sub-samplings, illustrated in Figure 3. Wavelet coefficients are computed at scales $2^j \leq 2^J$ and the lowest frequency image information is carried by the remaining averaged image $x \star \phi_J$. The convolution cascades (2) and (3) with h and g_θ can also be computed directly as convolutions with ϕ_j and $\psi_{j,\theta}$, using FFT's. For the sake of simplicity, we follow this second approach and thus specify directly the ϕ and ψ as opposed to the intermediate filters h and g_θ . We use a Morlet wavelet ψ and a Gaussian filter ϕ , further specified in [5]. The resulting wavelet transform W_1 is a contractive linear operator, which is nearly an isometry.

2.4. Roto-Translation Wavelet Transform W_2

Wavelet coefficients $|x \star \psi_{j,\theta}|$ are translation invariant only up to the scale 2^j . Increasing this invariance up to 2^J means further propagating these coefficients up to the last network layer J . This is be done by applying a second wavelet transform W_2 which is now defined. This second wavelet transform also recombines the output of wavelet filters along different angles. It thus also measures the angular variability of wavelet responses, as corner detectors.

At a depth j_1 , there are $\tilde{Q}_{j_1} = L$ wavelet image frames indexed by the angle $\theta = \ell\pi/L$ for $1 \leq \ell \leq L$:

$$x_{j_1}^1(p, \theta) = |x \star \psi_{j_1,\theta}(2^{j_1-1}p)|.$$

These coefficients are propagated to larger scales 2^j by computing convolutions and modulus with a new set of spatial wavelets $\psi_{j,\theta}(p)$ at larger scales $2^j > 2^{j_1}$.

As in deep convolution network architectures, we also recombine the information in these image frames indexed by the angle θ in (3). To understand how to do so, let us compute the wavelet coefficients of a rotated image $x_\alpha(p) = x(r_\alpha p)$ by an angle α :

$$x_\alpha \star \psi_{j_1,\theta}(p) = x \star \psi_{j_1,\theta-\alpha}(r_\alpha p).$$

It rotates the spatial coordinates p but also “translates” by α the angle parameter θ .

Our goal is not to build a rotation invariant representation but a representation which linearizes variabilites along rotation angles. These totation variabilities can thus be discriminated or removed by a linear classifiers at the output. We thus do not use a rotation invariant scattering representation as in [25]. To build a representation which is stable to rotations, and to deformations along rotations, we compute a wavelet transform along the angle parameter θ . It means performing convolutions along θ , with angular one-dimensional wavelets $\bar{\psi}_k(\theta) = 2^{-k} \bar{\psi}(2^{-k}\theta)$. The resulting wavelet transform W_2 computes separable convolutions along both the $2D$ spatial variable p and the angle variable θ , with a $3D$ separable complex wavelet defined by:

$$\psi_{j,\beta,k}(p, \theta) = \psi_{j,\beta}(p) \bar{\psi}_k(\theta).$$

It is a separable product of a spatial wavelet $\psi_{j,\beta}(p)$ of scale 2^j and an angular wavelet $\bar{\psi}_k(\theta)$ of scale 2^k for $1 \leq k \leq K < \log_2 L$. If $\bar{\psi}_k(\theta)$ are one-dimensional Morlet wavelets, then the resulting separable wavelet transform W_2 is a stable and invertible operator, which nearly preserves the signal norm.

The wavelet transform modulus for $j > j_1$ is computed with a three-dimensional separable convolution along the spatial and angular variables (p, θ) , and it performs a sub-sampling along both variables. It has a spatial scale 2^j and

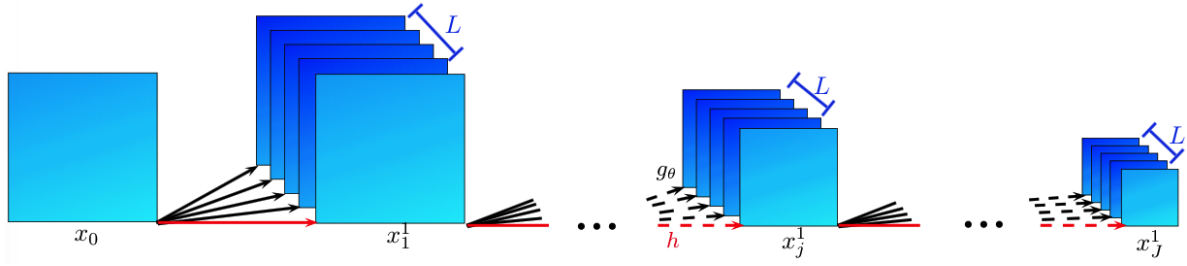


Figure 3. A wavelet modulus $|W_1|$ computes averages and modulus wavelet image frames at each layer x_j^1 , by cascading filtering, sub-sampling and modulus operators.

is thus stored at the layer j , via an index q which encodes θ , β , j_1 and the angular scale 2^k :

$$x_j^2(p, q) = |x_{j_1}^1 \star \psi_{j, \beta, k}(2^{-j-1}p, 2^{-k-1}\theta)|. \quad (4)$$

It propagates $x_{j_1}^1$ towards network layers of depth $j > j_1$, up to $j = J$. This 3D separable wavelet transform is either computed with a cascade of filtering across the deep network layers, or directly with 3D convolutions calculated with *FFT*'s.

For $j < J$, we still need to propagate the second order coefficients x_j^2 up to the largest spatial scale 2^J . This could be done by applying a third wavelet transform W_3 which could also enforce more complex geometric invariants by recombining information across angles and scales. In this implementation, we directly apply a linear averaging $x_j^2 \star \phi_J$ at the scale 2^J . It averages each image frame of x_j^2 with a spatial convolution with $\phi_J(p) = 2^{-2J} \phi(2^{-J}p)$.

The last layer x_J of this scattering network is an aggregation of the image x , of first order wavelet modulus images x_j^1 , and of second order coefficients x_j^2 at all scales $2^j \leq 2^J$, all of them averaged at the scale 2^J :

$$x_J = S_J x = \left\{ x \star \phi_J, x_j^1 \star \phi_J, x_j^2 \star \phi_J \right\}_{1 \leq j \leq J}.$$

First order coefficients $x_j^1 \star \phi_J$ are very similar to SIFT [19] feature vectors. They provide information on average energy distributions across scales and orientations over a neighborhood of size 2^J . A scattering representations can thus be interpreted as an “augmented” SIFT representation with second order coefficients $x_j^2 \star \phi_J$ providing information on interactions between scales and angles in multi-scale neighborhoods.

This deep scattering is computed by cascading the modulus $|W_1|$ of a first 2D spatial wavelet transform, followed by the modulus $|W_2|$ of a second 3D separable wavelet transform along space and angles, followed by the averaging $A_J z = z \star \phi_J$:

$$S_J x = A_J |W_2| |W_1| x.$$

Since W_1 and W_2 and A_J are contractive operators it guarantees that S_J is also contractive and hence stable to additive perturbations. Moreover, since the wavelet transforms

W_1 and W_2 and A_J are Lipschitz stable relatively to deformations [22], S_J is also Lipschitz and hence linearizes small deformations. This guaranties to avoid the instabilities observed on deep networks such as Alex-net [28] where a small image perturbation can considerably modify the network output and hence the classification.

For images of P pixels, each network layer x_j has Q_j image frames of $P_j = P 2^{-2j+2}$ pixels. For a gray level image such that $Q_0 = 1$, the resulting number of frames are respectively $Q_1 = 9$, $Q_2 = 145$, $Q_3 = 409$, $Q_4 = 801$, $Q_5 = 1321$, $Q_6 = 1969$, and $Q_j = 1 + Lj + L^2 j(j-1) \approx 64j^2$ when $j \gg 1$. Color images are represented by the three Y,U,V color bands, and each color band is decomposed independently. It thus multiplies the number of image frames Q_j by 3 for all $0 \leq j \leq J$. At the output layer J , the factor 2 spatial oversampling is removed so $P_J = P 2^{-2J}$. This last layer is thus an aggregation of $3P 2^{-2J}$ order 0 coefficients in $x \star \phi_J$, plus $3P 2^{-2J} L J$ order 1 coefficients in the $x_j^1 \star \phi_J$, and $3P 2^{-2J} L^2 J(J-1)$ order 2 coefficients in the $x_j^2 \star \phi_J$ arrays. For CalTech images of $P = 256^2$ pixels, decomposed with $J = 6$ scales and $L = 8$ angles, there are 48 order 0 coefficients, $2 \cdot 10^3$ order 1 coefficients, and $92 \cdot 10^3$ order 2 coefficients.

Good quality images can be reconstructed from scattering coefficients as long as the number of scattering coefficients is larger than the number of image pixels [4]. Despite the invariance to translation, the roto-translation scattering representation is thus nearly complete as long as $2^{-2J} L^2 J^2 \geq 1$. If $L = 8$ then it is valid for $J \geq 5$.

3. Supervised Feature Selection

The scattering representation has a number of coefficients which is of the same order as the original image. It provides a nearly complete signal representation, which allows one to build a very rich set of geometric invariants with linear projection operators. The choice of these linear projection operators is done at the supervised classification stage with an SVM. Scattering coefficients are strongly correlated. Results are improved by reducing the variance of the representation, with a supervised feature selection, which considerably reduces the number of scattering coef-

ficients before computing an SVM classifier. This is implemented with a supervised orthogonal least square regression [6, 1], which greedily selects coefficients with a regression algorithm.

A logarithm non-linearity is applied to scattering coefficients in order to separate low frequency multiplicative components due to the variations of illuminations. These low-frequency modulations add a constant to the logarithm of scattering coefficients which can then be removed with an appropriate linear projector by the final classifier. Also, it linearizes exponential decay of the scattering coefficients across scales.

In the following, we denote by $\Phi^1 x = \{\phi_p^1 x\}_p$ the logarithm of scattering coefficients at a scale 2^J . We are given a set of training images $\{x_i\}_i$ with their class label. The orthogonal least square selects a set of features adapted to each class C with a linear regression of the one-versus-all indicator function

$$f_C(x) = \begin{cases} 1 & \text{if } x \text{ belongs to class } C \\ 0 & \text{otherwise} \end{cases}.$$

It iteratively selects a feature in the dictionary and updates the dictionary. Let $\Phi^k x = \{\phi_p^k x\}_p$ be the dictionary at the k^{th} iteration. We select a feature $\phi_{p_k}^k x$, and we update the dictionary by decorrelating all dictionary vectors, relatively to this selected vector, over the training set $\{x_i\}_i$:

$$\tilde{\phi}_p^{k+1} = \phi_p^k - \left(\sum_i \phi_{p_k}^k(x_i) \phi_p^k(x_i) \right) \phi_{p_k}^k.$$

Each vector is then normalized

$$\phi_p^{k+1} = \tilde{\phi}_p^{k+1} \left(\sum_i |\tilde{\phi}_p^{k+1}(x_i)|^2 \right)^{-1}.$$

The k^{th} feature $\phi_{p_k}^k x$ is selected so that the linear regression of $f_C(x)$ on $\{\phi_{p_r}^k x\}_{1 \leq r \leq k}$ has a minimum mean-square error, computed on the training set. This is equivalent to finding $\phi_{p_k}^k$ in Φ^k which maximizes the correlation $\sum_i f_C(x_i) \phi_p^k(x_i)$.

The orthogonal least square regression thus selects and computes K scattering features $\{\phi_{p_k}^k x\}_{k < K}$ for each class C , which are linearly transformed into K decorrelated and normalized features $\{\phi_{p_k}^k x\}_{k < K}$. For a total of n_C classes, the union of all these feature defines a dictionary of size $M = K n_C$. They are linear combinations of the original log scattering coefficients $\{\phi_p x\}_p$. This dimension reduction can thus be interpreted as a last fully connected network layer, which outputs a vector of size M . The parameter M governs the bias versus variance trade-off. It can be adjusted from the decay of the regression error of each f_C or fixed a priori. In classification experiments, M is about 30 times smaller than the size of the original scattering dictionary.

The selected features are then provided to a Gaussian SVM classifier. The variance of the Gaussian kernel is set to the average norm of the scattering vectors, calculated from the training set. This large variance performs a relatively small localization in the feature space, but it reduces classification errors as shown in Table 1.

4. Image Classification Results

We compare the performance of a scattering network with state-of-the-art algorithms on CIFAR and Caltech datasets, which include complex object classes, at different or fixed resolutions.

Images of each databases are rescaled to become square images of 2^{2d} pixels. The scattering transform depends upon few parameters which are fixed a priori. The maximum scale of the scattering transform is set to $2^J = 2^{d-2}$. Scattering coefficients are thus averaged over spatial domains covering 1/4 of the image width, and coefficients sampled over a spatial grid of 4×4 points, a final down-sampling being performed without degrading classification accuracies. This preserves some coarse localization information. Coefficients are computed with Morlet wavelets having $L = 8$ orientations. The wavelet transform along these $L = 8$ angles are computed at a maximum scale $2^K = L/2$, which corresponds to a maximum angular variation of $\pi/2$. Indeed these object recognition problems do not involve larger rotation variability. The resulting scattering representation is nearly complete as previously explained. It is computed independently along the 3 color channels YUV. We apply a logarithm to separate illumination components. The classifier is implemented by first reducing the dimensionality, to $M = 2000$ feature vectors on CIFAR-10 for instance, with an orthogonal least square regression, and applying a Gaussian SVM. We use the same architecture and same hyperparameters for each dataset, apart from the number M of selected coefficients, which increases proportionally to the size of the scattering representation, which depends upon the image size.

Caltech-101 and Caltech-256 are two color image databases, with respectively 101 and 256 classes. They have 30 images per class for training and the rest is used for testing. Caltech images are rescaled to square images of $P = 2^{2d} = 256^2$ pixels. Average per class classification results are reported with an averaging over 5 random splits. We removed the clutter class both from our training and testing set.

CIFAR are more challenging color image databases due to its high class variabilities, with 60000 tiny colors images of $P = 2^{2d} = 32^2$ pixels. CIFAR-10 has 10 classes with 5000 training images per class, whereas CIFAR-100 has 100 classes with 500 training images per class.

Table 1 gives the classification accuracy for different scattering configurations, on the datasets CIFAR-10 and

Scattering	Caltech-101	CIFAR-10
Trans., order 1	59.8	72.6
Trans., order 2	70.0	80.3
Trans., order 2 + OLS	75.4	81.6
Roto-Trans., order 2	74.5	81.5
Roto-Trans., order 2 + OLS	79.9	82.3

Table 1. Classification accuracy with 5 scattering configurations. First a translation scattering up to order 1, then up to order 2, then withan Orthogonal Least Square (OLS) feature reduction. Then a roto-translation scattering up to order 2, then with an OLS feature reduction.

Caltech-101. First order scattering coefficients are comparable to SIFT [5], but are calculated over larger neighborhoods. Second order scattering coefficients computed with translated wavelets (no filtering along rotations) reduces the error by 10%, which shows the importance of this complementary information. Incorporating a wavelet filtering along rotations as in Section 2, leads to a further improvement of 4.5% on Caltech-101 and 1.2% on CIFAR-10. Rotations produce larger pixel displacements on higher resolution images. It may explain why improving sensitivity to rotations plays a more important role on Caltech images, which are larger. Adding a feature reduction by orthogonal least square reduces the error by 5.4% on Caltech-101 and 0.7% on CIFAR-10. The orthogonal least square has a bigger impact on Caltech-101 because there are less training examples per class, so reducing the variance of the estimation has a bigger effect.

Tables 2,3,4,5 report the classification accuracy of a second order roto-translation scattering algorithm with an orthogonal least square feature selection, for CIFAR and Caltech databases. It is compared to state of the art algorithms, divided in four categories. “Prior” feature algorithms apply a linear or an RBF type classifier to a predefined set of features, which are not computed from training data. Scattering, SIFT and HOG vectors, or deep networks with random weights belong to this Prior class. “Unsup. Deep” algorithms correspond to unsupervised convolutional deep learning algorithms, whose filters are optimized with non-labeled training data, before applying a linear classifier or a Gaussian kernel SVM. “Unsup. Dict.” algorithms transform SIFT type feature vectors or normalized pixel patches, with one, two or three successive sparse dictionaries computed by unsupervised learning. It may then be followed by a max-pooling operator over a pyramid structure [12]. To normalize unsupervised learning experiments, we only consider results obtained without data augmentation. “Supervised” algorithms compute feature or kernel representations, which are optimized with supervised learning over labeled training data. In this case, the training may be performed on a different databasis such as ImageNet, or may

include a data augmentation by increasing the dataset with affine transformations and deformations. Supervised deep convolution networks or supervised kernel learning are examples of such algorithms.

Scattering gives better classification results than all prior feature classification on Caltech-101, as shown by Table 2. Convolutional network with random filters on mono-CIFAR-10 (gray level CIFAR-10) have an accuracy of 53.2% in [24]. Color information improves classification results by at most 10% on all algorithms, so it remains well below scattering accuracy. No result is reported on CIFAR-100 using predefined “prior” feature classifiers. Tables 2 and 4 shows that scattering networks performs at least as well as unsupervised deep convolutional architectures without data augmentation on Caltech-101 and CIFAR-10. To our knowledge, no result with unsupervised deep convolutional network learning have been reported on Caltech-256.

State-of-the-art unsupervised classification results for Caltech, without data augmentation, are obtained with a Multipath-SC algorithm [2], which has 3 unsupervised encoding layers. Similar results are obtained with Spatial Local Coding descriptors [23] with a first layer of nearly SIFT descriptors followed by an unsupervised coding and multi-scale pyramidal pooling. Caltech-101 is an easier data basis because it has a bias across classes, which is typically used by classifiers. This bias is removed from Caltech 256 which explains why classifiers have a lower accuracy. The unsupervised classification algorithm reporting state of the art results on CIFAR are different from the one on Caltech, which shows that these figures must be analyzed with precaution. The scattering classifier gives comparable with all unsupervised algorithms on CIFAR-10 and CIFAR-100.

Let us emphasize that we are using the same scattering representation, besides image size adaptation, for Caltech and CIFAR databases. RFL [10] is the only unsupervised learning algorithm which reports close to state of the art results, both on Caltech and CIFAR data bases. RFL does not perform as well as a scattering on Caltech and CIFAR-100, and slightly better on CIFAR-10. This illustrates the difficulty to have a single algorithm which works efficiently on very different databases. We reported the result on CIFAR-100 from [10] via [20].

The best classification results are obtained by supervised deep convolutional networks [16, 9, 30]. They improve non-supervised accuracy by about 10% on CIFAR-10 or Caltech-101, 20% on Caltech-256, but 5% on CIFAR-100. The improvement on CIFAR-100 is smaller than on CIFAR-10 because there is only 500 samples per classes for supervised training, as opposed to 5000. The Caltech data bases does not have enough training sample to train a supervised deep network. We thus report classification results obtained by the supervised Alex-network trained on ImageNet, to which is applied a linear SVM classifier which

Method	Type	Accuracy
RotoTrans. Scat.	Prior	79.9
Random Filters [15]	Prior	62.9
CDBN [17]	Unsup. Deep	65.4
M-HMP[2]	Unsup. Dict	82.5
SLC [23]	Unsup. Dict	81.0
Ask the locals [3]	Unsup. Dict	77.3
RFL [10]	Unsup. Dict	75.3
CNN [9]	Supervised	91.4

Table 2. Results for different types of representations on Caltech-101.

Method	Type	Accuracy
RotoTrans. Scat.	Prior	43.6
M-HMP [2]	Unsup. Dict	50.7
SLC [23]	Unsup. Dict	46.6
Ask the locals [3]	Unsup. Dict	41.7
CNN [30]	Supervised	70.6

Table 3. Results for different types of representations on Caltech-256.

Method	Type	Accuracy
RotoTrans. Scat.	Prior	82.3
RFL [10]	Unsup. Dict	83.1
NOMP [18]	Unsup. Dict	82.9
LIFT [27]	Unsup. Deep	82.2
CNN [16]	Supervised	91.8

Table 4. Results for different types of representations on CIFAR-10.

Method	Type	Accuracy
RotoTrans. Scat.	Prior	56.8
RFL [10]	Unsup. Dict	54.2
NOMP [18]	Unsup. Dict	60.8
CNN [16]	Supervised	65.4

Table 5. Results for different types of representations on CIFAR-100.

is trained on Caltech [8]. Although this deep network was not trained on Caltech, it still achieves the state of the art on this databases. Experiments show that if the training and testing image datasets are different, a supervised deep network provides a feature vector having a lower accuracy for classification, but this accuracy is not dramatically reduced. It indicates that supervised deep classifiers are learning generic image representations which are likely to capture more complex geometric properties than unsupervised algorithms or a roto-translation scattering transform.

A scattering transform is computed with convolutions along groups of transformations which create important im-

age variability. This paper concentrates on translations and rotations, but it can be extended to any other group. Improving results requires to consider other source of variabilities and invariants, for example across color channels or across scales, which are not recombined in this architecture. Supervised deep neural networks do apply non-linear transformations across color bands and scales. Computing wavelet and scattering transforms on arbitrary Lie groups or finite groups is not difficult [22]. What is harder is to identify the important group of variability for improving classification. It seems that supervised deep network classifiers are able to identify them.

5. Conclusion

This work shows that feature vectors for image classification can be constructed from geometric image properties as opposed to learning. A roto-translation scattering transform constructs a feature vector providing joint information along multiple scales and multiple angles. For complex object classification problems as in Caltech and CIFAR databases, it considerably improves the performance of all existing prior image descriptors, and it yields comparable results with state of the art unsupervised deep learning, and dictionary learning algorithms.

Scattering networks do not have instability properties as the ones observed for Alex-net [28], because it applies contractive wavelet operators which are stable to deformations. However, deep neural networks with supervised training provide a clear improvement of average classification accuracy, compared to unsupervised learning and to this roto-translation scattering transform. This may indicate that they capture refined but important geometric image properties. Understanding the nature of these properties is an open challenge to further improve the performances of scattering representations.

Acknowledgments

This work is funded by the ERC grant InvariantClass 320959 and via a grant for Phd Students of the Conseil régional d’Île-de-France (RDM-IdF).

References

- [1] T. Blumensath and M. E. Davies. On the difference between orthogonal matching pursuit and orthogonal least squares. 2007. 6
- [2] L. Bo, X. Ren, and D. Fox. Multipath Sparse Coding Using Hierarchical Matching Pursuit. In *CVPR*, pages 660–667. IEEE, 2013. 7, 8
- [3] Y.-L. Boureau, N. L. Roux, F. Bach, J. Ponce, and Y. LeCun. Ask the locals: Multi-way local pooling for image recognition. In D. N. Metaxas, L. Quan, A. Sanfeliu, and L. J. V. Gool, editors, *ICCV*, pages 2651–2658. IEEE, 2011. 8

- [4] J. Bruna. Signal and Texture Recovery from Scattering Representations. 2014. [1](#), [5](#)
- [5] J. Bruna and S. Mallat. Invariant Scattering Convolution Networks. *IEEE Trans. Pattern Anal. Mach. Intell.*, 35(8):1872–1886, 2013. [1](#), [3](#), [4](#), [7](#)
- [6] S. Chen, C. F. Cowan, and P. M. Grant. Orthogonal least squares learning algorithm for radial basis function networks. *Neural Networks, IEEE Transactions on*, 2(2):302–309, 1991. [6](#)
- [7] N. Dalal and B. Triggs. Histograms of oriented gradients for human detection. In *Computer Vision and Pattern Recognition, 2005. CVPR 2005. IEEE Computer Society Conference on*, volume 1, pages 886–893. IEEE, 2005. [1](#), [8](#)
- [8] R. B. Girshick, J. Donahue, T. Darrell, and J. Malik. Rich feature hierarchies for accurate object detection and semantic segmentation. *CoRR*, abs/1311.2524, 2013. [1](#), [8](#)
- [9] K. He, X. Zhang, S. Ren, and J. Sun. Spatial pyramid pooling in deep convolutional networks for visual recognition. In *Computer Vision—ECCV 2014*, pages 346–361. Springer, 2014. [7](#), [8](#)
- [10] Y. Jia, C. Huang, and T. Darrell. Beyond spatial pyramids: Receptive field learning for pooled image features. In *CVPR*, pages 3370–3377. IEEE, 2012. [7](#), [8](#)
- [11] A. Krizhevsky, I. Sutskever, and G. E. Hinton. ImageNet Classification with Deep Convolutional Neural Networks. In P. L. Bartlett, F. C. N. Pereira, C. J. C. Burges, L. Bottou, and K. Q. Weinberger, editors, *NIPS*, pages 1106–1114, 2012. [1](#), [2](#)
- [12] S. Lazebnik, C. Schmid, and J. Ponce. Beyond Bags of Features: Spatial Pyramid Matching for Recognizing Natural Scene Categories. In *CVPR (2)*, pages 2169–2178. IEEE Computer Society, 2006. [1](#), [7](#)
- [13] Q. V. Le, M. Ranzato, R. Monga, M. Devin, G. Corrado, K. Chen, J. Dean, and A. Y. Ng. Building high-level features using large scale unsupervised learning. In *ICML*. icml.cc / Omnipress, 2012. [1](#)
- [14] Y. Lecun, B. Boser, J. S. Denker, D. Henderson, R. E. Howard, W. Hubbard, and L. D. Jackel. Back-Propagation Applied to Handwritten Zip Code Recognition. *Neural Computation*, 1(4):541–551, 1989. [2](#)
- [15] Y. LeCun, K. Kavukcuoglu, and C. Farabet. Convolutional networks and applications in vision. In *ISCAS*, pages 253–256. IEEE, 2010. [2](#), [8](#)
- [16] C.-Y. Lee, S. Xie, P. Gallagher, Z. Zhang, and Z. Tu. Deeply-Supervised Nets. *arXiv preprint arXiv:1409.5185*, 2014. [1](#), [7](#), [8](#)
- [17] H. Lee, R. B. Grosse, R. Ranganath, and A. Y. Ng. Convolutional deep belief networks for scalable unsupervised learning of hierarchical representations. In A. P. Danyluk, L. Bottou, and M. L. Littman, editors, *ICML*, volume 382 of *ACM International Conference Proceeding Series*, page 77. ACM, 2009. [8](#)
- [18] T.-H. Lin and H. EDU. Stable and Efficient Representation Learning with Nonnegativity Constraints. [8](#)
- [19] D. Lowe. Distinctive image features from scale-invariant key-points. *Intl. Journal of Computer Vision*, 60:91–110, 2004. [1](#), [5](#)
- [20] M. Malinowski and M. Fritz. Learning smooth pooling regions for visual recognition. In *the British Machine Vision Conference*, 2013. [7](#)
- [21] S. Mallat. *A Wavelet Tour of Signal Processing*. San Diego : Academic Press, 1999. [3](#)
- [22] S. Mallat. Group Invariant Scattering. *CoRR*, abs/1101.2286, 2011. [1](#), [2](#), [3](#), [5](#), [8](#)
- [23] S. McCann and D. G. Lowe. Spatially Local Coding for Object Recognition. In K. M. Lee, Y. Matsushita, J. M. Rehg, and Z. Hu, editors, *ACCV (1)*, volume 7724 of *Lecture Notes in Computer Science*, pages 204–217. Springer, 2012. [7](#), [8](#)
- [24] A. M. Saxe, P. W. Koh, Z. Chen, M. Bhand, B. Suresh, and A. Y. Ng. On Random Weights and Unsupervised Feature Learning. In L. Getoor and T. Scheffer, editors, *ICML*, pages 1089–1096. Omnipress, 2011. [2](#), [7](#)
- [25] L. Sifre and S. Mallat. Rotation, Scaling and Deformation Invariant Scattering for Texture Discrimination. In *CVPR*, pages 1233–1240. IEEE, 2013. [1](#), [3](#), [4](#)
- [26] J. Sivic, B. C. Russell, A. A. Efros, A. Zisserman, and W. T. Freeman. Discovering objects and their location in images. volume 1, pages 370–377, 2005. [1](#)
- [27] K. Sohn and H. Lee. Learning Invariant Representations with Local Transformations. In *ICML*. icml.cc / Omnipress, 2012. [8](#)
- [28] C. Szegedy, W. Zaremba, I. Sutskever, J. Bruna, D. Erhan, I. J. Goodfellow, and R. Fergus. Intriguing properties of neural networks. *CoRR*, abs/1312.6199, 2013. [2](#), [5](#), [8](#)
- [29] P. Vincent, H. Larochelle, Y. Bengio, and P.-A. Manzagol. Extracting and composing robust features with denoising autoencoders. In W. W. Cohen, A. McCallum, and S. T. Roweis, editors, *ICML*, volume 307 of *ACM International Conference Proceeding Series*, pages 1096–1103. ACM, 2008. [2](#)
- [30] M. D. Zeiler and R. Fergus. Visualizing and Understanding Convolutional Networks. *CoRR*, abs/1311.2901, 2013. [1](#), [7](#), [8](#)